Phys Chem Minerals (2006) 33: 256–265
DOI 10.1007/s00269-006-0074-1

ORIGINAL PAPER

J. M. Brown · E. H. Abramson · R. J. Angel

Triclinic elastic constants for low albite

Received: 14 September 2005 / Accepted: 16 February 2006 / Published online: 21 March 2006

Abstract The full set of elastic constants for plagioclase end-member phase albite ($NaAlSi_3O_8$) is reported for the first time. Velocities of surface acoustic waves (both Rayleigh and pseudo-surface waves) were measured using impulsively stimulated light scattering on polished surfaces having six different orientations (three normal to the Cartesian axes and three lying on diagonals). Data were inverted and results tested using several non-linear optimization techniques. Compliance moduli determined under hydrostatic compression provided additional constraints and reduced covariance in the reported constants. The Cartesian coordinate system associated with the constants (using the $C\bar{1}$ unit cell) has the *y*-axis parallel to the crystal *b* axis, the *x*-axis parallel to a* (perpendicular to *b* and *c*) and the *z*-axis consistent with a right-handed coordinate system. The values of the moduli C_{11}, C_{12}, C_{13}, C_{14}, C_{15}, C_{16}, C_{22}, C_{23}, C_{24}, C_{25}, C_{26}, C_{33}, C_{34}, C_{35}, C_{36}, C_{44}, C_{45}, C_{46}, C_{55}, C_{56}, C_{66} and their 2σ uncertainties (in parentheses) are, respectively, 69.1(0.6), 34.0(0.7), 30.8(0.5), 5.1(0.1), −2.4(0.1), −0.9(0.1), 183.5(2.7), 5.5(2.2), −3.9(0.5), −7.7(0.7), −5.8(0.7), 179.5(2.3), −8.7(0.4), 7.1(0.6), −9.8(0.6), 24.9(0.1), −2.4(0.1), −7.2(0.1), 26.8 (0.2), 0.5(0.1), 33.5(0.2). These constants differ significantly from the previously reported pseudo-monoclinic constants that were based on velocity measurements on polysynthetic twinned crystal aggregates. Differences are consistent with systematic errors in the earlier study associated with sparse data and the presence of cracks and other imperfections.

J. M. Brown (✉) · E. H. Abramson
Department of Earth and Space Sciences,
University of Washington, Box 351310, Seattle
WA 98195, USA
E-mail: brown@ess.washington.edu
Tel.: +1-206-6166058

R. J. Angel
Department of Geosciences, Virginia Tech,
Virginia Tech Crystallography Laboratory,
Blacksburg, VA 24060, USA

Introduction

Feldspars are the most abundant mineral group found in Earth's crust (estimated to constitute more than 60% of the crust). Albite ($NaAlSi_3O_8$) anchors the two main feldspar compositional series: the alkali feldspars (Na,K) $AlSi_3O_8$ and the plagioclase series (Na,Ca)Al(Si,Al) Si_2O_8. Albite has triclinic symmetry ($C\bar{1}$), which is common for the "low temperature" alkali-feldspar and albite-rich plagioclase with ordered aluminum and silicon in the tetrahedral sites.

Efforts to understand the structure and composition of the deep crust require interpretation of seismic data using mineral elastic constants. The existing and pioneering feldspar elasticity data, reported by Ryzhova (1964), were based on one-bar studies of pseudo-monoclinic crystal aggregates rather than on studies of true single crystals. Polysynthetic twinning in feldspars is ubiquitous and the two common twin laws (pericline and albite) increase the ensemble symmetry from triclinic (requiring 21 elastic constants) to monoclinic (13 elastic constants). Ryzhova's results are widely cited in handbooks and databases (e.g. Every and McCurdy 1992; Bass 1995; Hacker and Abers 2004). All subsequent efforts to model seismic properties of the crust have relied on these data (e.g. Peselnick et al. 1974; Liebermann and Ringwood 1976; Christensen and Fountain 1975; Salisbury and Christensen 1978; Babuska 1981; McDonough and Fountain 1988; Fountain et al. 1990; Seront et al. 1993; Salisbury and Fountain 1994; Christensen 1996; Takanashi et al. 2001; Hacker et al. 2003; Carlson and Miller 2004).

We measured velocities of surface waves in low albite (with full aluminum/silicon ordering) using impulsively stimulated light scattering (ISLS) and inverted the data to determine elastic constants. Compliance moduli determined under hydrostatic compression serve as additional constraints in the inversion. The resulting constants provide the first full triclinic set reported for any mineral; only two other triclinic crystals have ever

been characterized (Haussuhl and Siegert 1969; Kuppers and Siegert 1970). The new constants are significantly different than the previously reported monoclinic pseudo-single crystal properties. We reappraise methodology in the earlier experiments and find that the data acquisition scheme was not adequate to constrain even monoclinic constants. We also suspect that cracks in the polycrystalline aggregate resulted in underestimates of the true single crystal properties. An appendix defines the contracted Voigt notation used in this paper.

Prior ultrasonic elasticity determinations

Ryzhova (1964) reported ultrasonic velocities in heavily twinned plagioclases for three wave-vector polarizations, measured in six (Cartesian) propagation directions [(100) (001) (010) (110) (101) and (011)] for five plagioclase compositions ranging from An_9 to An_{56} (as measured along the albite-anorthite compositional join with pure albite being An_0). A later paper (Aleksandrov et al. 1974) reanalyzed the same data. Monoclinic elastic constants reported in both papers for An_9 are given in Table 1.

Ryzhova noted that although velocities were measured with a precision of 1.5%, actual measurements had a "spread (up to 5%)" associated with "errors in orientation and imperfections in the crystal itself: cracks, pores, and inclusions". No estimates of uncertainties of the elastic constants were given in either the 1964 or 1974 papers. Velocity data and velocities calculated using the 1964 and 1974 elastic constants for An_9 are shown in Fig. 1 (along with velocities calculated from a monoclinic average of the current results). Velocities calculated using Ryzhova's or Aleksandrov's constants reproduce most of the data within the stipulated 5% error bars; a few points misfit by as much as 10%.

Formal uncertainties (e.g. Brown et al. 1989), of the monoclinic elastic constants, calculated here based on the statistics of Ryzhova's data acquisition scheme are given in Table 1. Accepting Ryzhova's estimate, we use an uncertainty of 1.5% for velocity measurements. It is clear that the 18 reported velocities do not adequately constrain 13 monoclinic elastic constants. In particular, the constants C_{12}, C_{23} and C_{25} which differ most between the 1964 and 1974 analyses have large mutual covariance and, as a result, large individual uncertainties.

In a study of velocities measured in a plagioclase aggregate of intermediate composition, Seront et al. (1993) noted that hydrostatic pressure of 1 GPa is necessary to close cracks. Associated with crack closure, differences in velocities between 1 bar and 1 GPa can be greater than 10% (intrinsic pressure derivatives of the

Table 1 Elastic constants and 2σ uncertainties for albite in units of GPa

	Ryzhova	Aleksandrov et al.	Uncertainties	Ryzhova rotated	Current results	Uncertainties	Uncertainties
11	74.9	74.8	6.0	66.8	69.9	0.6	3.1
12	36.3	28.9	> 50	27.2	34.0	0.7	5.7
13	37.6	38.1	12.2	34.0	30.8	0.5	4.2
15	−9.1	−9.1	9.7	0.1	−2.4	0.1	0.6
22	137.5	137.4	8.8	137.5	183.5	2.7	13.3
23	32.6	21.5	> 50	41.7	5.5	2.2	6.5
25	−10.4	−30.7	> 50	−7.7	−7.7	0.7	1.2
33	128.9	128.8	8.4	144.3	179.5	2.3	7.1
35	−19.1	−19.2	9.9	4.7	7.1	0.6	1.2
44	17.2	17.4	1.1	22.5	24.9	0.1	0.2
46	−1.3	−2.1	3.9	−7.4	−7.2	0.1	0.1
55	30.3	30.2	4.0	26.7	26.8	0.2	0.2
66	31.1	31.8	1.6	25.8	33.5	0.2	0.2
14					5.1	0.1	0.4
16					−0.9	0.1	1.1
24					−3.9	0.5	0.9
26					−5.8	0.7	2.6
34					−8.7	0.4	0.8
36					−9.8	0.6	1.2
45					−2.4	0.1	0.1
56					0.5	0.1	0.2

The first column lists the constant subscripts using Voigt notation. The first 13 constants are required for both monoclinic and triclinic crystals, but the last 8 constants are only non-zero in triclinic crystals. The second column lists the elastic constants reported by Ryzhova (1964). The third column lists the elastic constants reported by Aleksandrov et al. (1974). The fourth column lists the formal uncertainties (2σ) for columns 2 and 3 assuming 1.5% uncertainty in velocities. The calculated uncertainties for three constants are numerically unstable since data do not provide an adequate constraint. The fifth column lists elastic constants reported by Ryzhova rotated into the coordinate system used in this paper. The sixth column lists the current results. The seventh column lists the formal uncertainties (2σ) for the current study and the eight column lists the formal uncertainties (2σ) for the current study without the constraints provided by the x-ray compression data

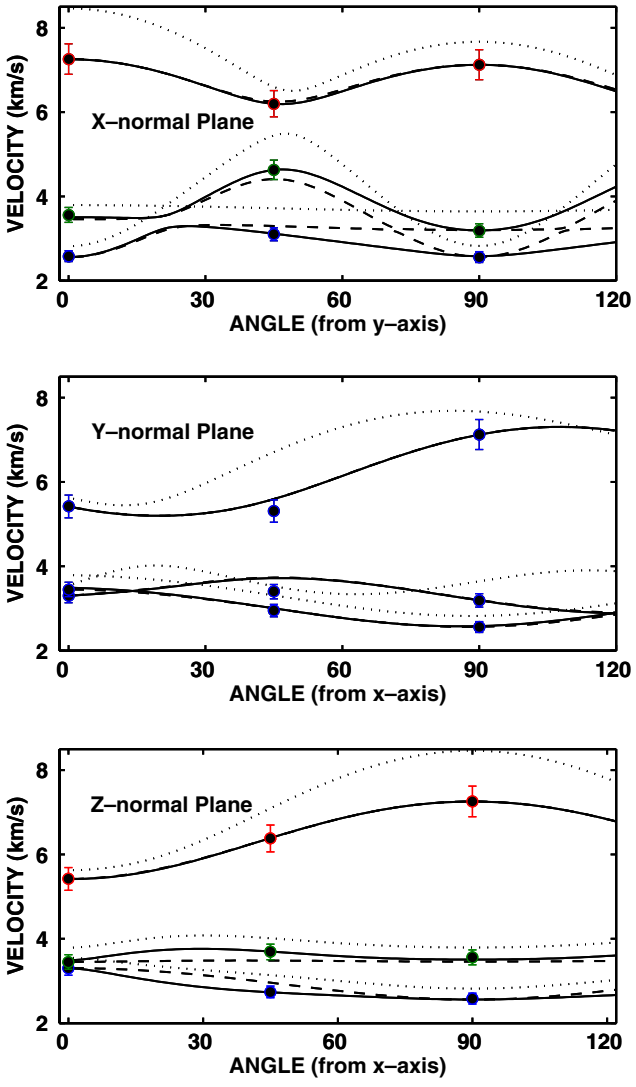

Fig. 1 Ultrasonic body wave velocities measured and predicted within three orthogonal planes through a polysynthetic twinned aggregate of An_9 composition. Measured velocities and error bars are from Ryzhova (1964). The *curves* are as predicted by constants given by Ryzhova (*dashed*), Aleksandrov et al. (1974) (*solid*), and current work (*dotted*). The *dashed and solid curves* coincide over most of the plotted range

elastic constants are relatively small). Seront et al. calculated velocities using averaged elastic constants based on measured lattice-preferred orientations of the constituent minerals and suggested that Ryzhova's elastic constants are low by approximately 10%.

In summary, prior velocity data for albite are not adequate for a correct determination of the elastic constants. Several monoclinic constants are essentially unconstrained by the sparse data, experimental errors were large, and the reported presence of cracks suggests that measured velocities were lower than would be the case in a crack-free, single crystal. Although widely cited, elastic constants calculated on the basis of those measurements are of questionable validity.

X-ray compression measurements

Benusa et al. (2005) used x-ray diffraction to determine the compression of a single crystal of low albite under hydrostatic pressure. The precision of the data is sufficient to determine six independent values of the linearized Lagrangian finite strain tensor (L_i in Voigt notation) (Schlenker et al. 1978), which are induced by each increment in pressure and thus determine six independent combinations of elastic compliances $S_{ij} = \text{inv}(C_{ij})$ (Fig. 2). Implicit is the assumption that experimental strain increments are sufficiently small such that $L_i/\Delta P$ is equal to the appropriate sums of the elastic compliances. Extrapolated to $P=0$, these sums of compliances are used as additional constraints in our fit of the velocity data. The values are given in Table 2 and compared both with those given by our final fits as calculated from the constants suggested by Ryzhova. In further support of the conclusion of Seront et al. (1993), compliances predicted from Ryzhova's constants are generally too large; $L_2/\Delta P$ and $L_5/\Delta P$ are significantly over-estimated.

The sums of (isothermal) compliances determined by the x-ray data can be used in the inversion of (adiabatic) velocity data only after conversion from isothermal to adiabatic values. The additive correction (Nye 1969) to the isothermal S_{ij} is $\alpha_i\alpha_j T/C_p$ where α_i denotes the thermal expansivity tensor (Voigt notation) and C_p the heat capacity per unit volume. The α_i = (17, 4.5, 0.5, 5, 5, 5)$\times 10^{-6}$ K^{-1} is determined from x-ray data taken between 25 and 970°C (Winters et al. 1979) as $L_i/\Delta T$, analogously to the previous determination of the sums of elastic compliances, while $C_p = 2.08\times 10^6$ J m^{-3} K^{-1} (Navrotsky 1995). In the case of albite, these corrections turn out to be less than 1% of the values given in Table 2, far smaller than the associated experimental uncertainties and are thus negligible in the current analysis.

Sample characterization

We use single crystals collected by B. Evans in central Crete (near Therison) from a vein in a blueschist terrain. The samples are several millimeters in size with euhedral and fractured surfaces. They are clear, with no obvious twinning. Some samples have actinolite inclusions. Microprobe analyses confirmed end-member albite stochiometery. Cations other than sodium, aluminum and silicon were beneath detection thresholds (< 0.05 wt% for CaO and K_2O). The x-ray determination of unit-cell parameters in the $C\bar{1}$ unit-cell setting [a = 8.13662(2)Å, b = 12.7857(2)Å, c = 7.1582(3)Å] and angles [α = 94.253(2)°, β = 116.605(2)°, γ = 87.756(2)°] are in agreement with literature values for endmember low albite (Harlow and Brown 1980; Downs and Hall-Wallace 2003). A structure determination from a small fragment of the sample gave mean

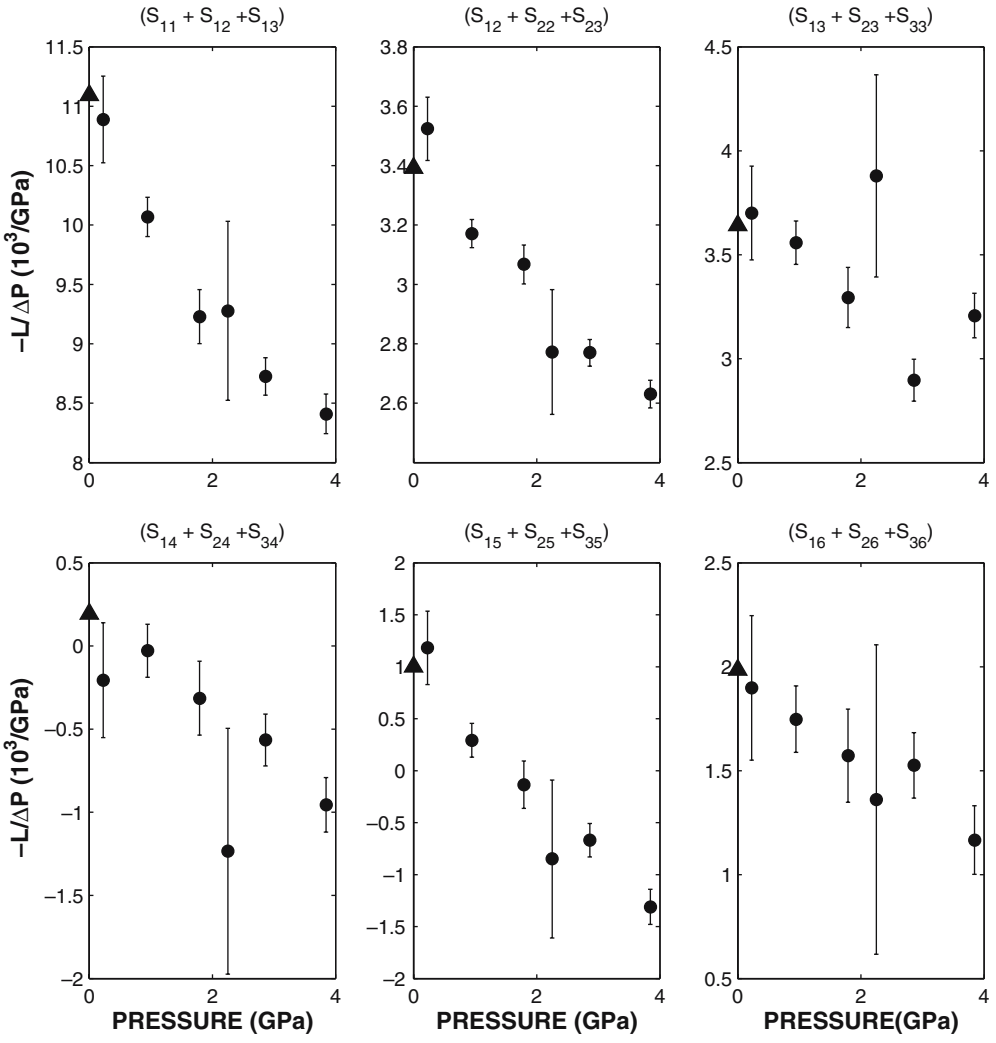

Fig. 2 Each of six different sums of compliances, calculated from the x-ray differential strain measurements at each increment of pressure, are plotted against the mean pressure for each increment. *Triangles* are the sums of compliances from the current set of 1 bar elastic constants

bond lengths <T-O> for the tetrahedral cation sites of <T1o-O> = 1.741 Å, <T1m-O> = 1.611 Å, <T2o-O> = 1.616 Å and <T2m-O> = 1.617 Å. These correspond to a fully-ordered Al, Si distribution, within the uncertainties of the measurement (Kroll and Ribbe 1983). The calculated density is 2.623(3) g cm^{-3}.

We chose the following convention to align the non-orthogonal crystal axes with respect to Cartesian coordinates. The *y*-axis is aligned parallel to the crystal *b*-axis. The *x*-axis is set in the a* direction (perpendicular to the *b*- and *c*-axes). The *z*-axis is chosen to satisfy a right-handed coordinate system. This convention is different from that used by Ryzhova who also set the *y*-axis parallel to *b*, but then set the *z*-axis parallel to c*. Relative to our system, these coordinates are rotated 26.6° about the *b*-axis. Although Ryzhova's convention was motivated by the nature of the underlying crystal structure (placing the crankshaft chain structure of

Table 2 Sums of compliances (GPa^{-1}), as predicted by the data of Benusa et al. (2005) (extrapolated to $P = 0$), by Ryzhova's (1964) constants, and by current work

	Benusa et al.	Ryzhova	Current work
$L_1/\Delta P = S_{11} + S_{12} + S_{13}$ (GPa^{-1}) × 1e3	11.1 (0.2)	11.5	11.1
$L_2/\Delta P = S_{21} + S_{22} + S_{23}$ (GPa^{-1}) × 1e3	3.4 (0.2)	4.1	3.4
$L_3/\Delta P = S_{31} + S_{32} + S_{33}$ (GPa^{-1}) × 1e3	3.8 (0.2)	3.5	3.6
$L_4/\Delta P = S_{41} + S_{42} + S_{43}$ (GPa^{-1}) × 1e3	0.0 (0.2)	–	0.2
$L_5/\Delta P = S_{51} + S_{52} + S_{53}$ (GPa^{-1}) × 1e3	1.0 (0.2)	3.7	1.0
$L_6/\Delta P = S_{61} + S_{62} + S_{63}$ (GPa^{-1}) × 1e3	2.0 (0.2)	–	2.0

Components of the strain tensor L and compliances S are given in standard Voigt notation. Two of the strains (L_4 and L_6) are zero in the case of monoclinic symmetry

albite parallel to the x-axis), it results in compressional velocities in the x–z plane which enjoy no simple relationship to the Cartesian coordinates. With the convention used here, maxima and minima of the compressional velocities lie close to the coordinate axes, with values determined by the constants C_{11}, C_{22}, and C_{33}.

Samples were oriented on an x-ray diffractometer. Crystals, in selected orientations, were glued to a glass slide while still attached to the x-ray goniometer head. The samples were subsequently ground flat using 0.25 micron diamond grit for the final polish. Forty nanometer (± 5 nm) of aluminum was deposited on the polished surfaces. This metallic layer allows the coupling of the incident laser energy to the surface of the crystal and the resulting generation of surface waves.

Six planar cuts through the albite samples were prepared. Directions of propagation along the sample surfaces are shown in a stereographic perspective in Fig. 3. Three cuts were essentially normal to the Cartesian axes, the other three being cross-cutting diagonal slices.

Experimental method

The general experimental method (ISLS) has been described elsewhere [see Abramson et al. (1999) for a general review]. Both body wave and surface wave velocities have been reported and elastic constants of crystals at ambient pressure and at high pressure have been determined. In brief, two 100 ps pulses are selected from the pulse train of a Nd:YAG laser (of wavelength $\lambda_{IR} = 1{,}064$ nm) and combined at an angle, intersecting on the sample surface to form a one-dimensional interference pattern filling a spot of ~300 μm diameter. Energy is absorbed in the thin, overlying, aluminum film, creating a spatially periodic variation in surface temperature. Rapid thermal expansion creates a surface corrugation and launches surface acoustic waves (SAW). The acoustic wavelength λ_A (~2.55 μm) is that of the interference pattern: $\lambda_A = \lambda_{IR}/2/\sin\Theta$, where Θ is half the angle of intersection of the two pulses.

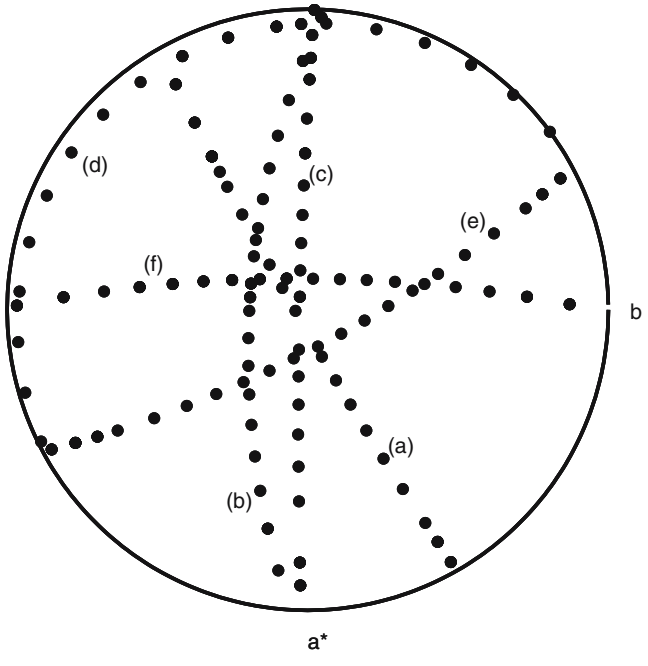

Fig. 3 Equal area stereographic projection of propagation directions of surface waves for the data reported here. Data were nominally collected at 10° increments over 180° on six polished surfaces [labeled (**a**) through (**f**), corresponding to the order of data sets shown in Fig. 5]

The SAW causes temporally and spatially periodic changes in the sample surface, which can diffract a probe beam. A third pulse is selected from the Nd:YAG laser, frequency doubled to 532 nm, and delayed by time of flight to create the probe. The intensity of the acoustically diffracted portion of the probe is recorded as a function of delay time and this signal is then Fourier transformed to determine the frequencies of the SAWs. For an acoustic frequency f_A and the wavelength λ_A, the velocity is $V = \lambda_A f_A$. Rotation of each sample about its surface normal allows waves to be launched, and velocities measured, in any direction contained in the plane.

We measured SAW velocities (both pure Rayleigh and pseudo-surface waves) on the oriented and polished single crystals. Velocities were measured with a reproducibility of about 0.2%. An absolute accuracy of about 0.1% is estimated on the basis of uncertainties in the velocity of our standard (which is calibrated relative to measurements of the velocity of water). The aluminum film on the samples alters surface wave velocities by about 0.1%; this systematic effect is included in the data analysis. Although care was taken to accurately determine propagation directions, the mechanical steps necessary to transfer an x-ray orientation to the optics table rotation stage resulted in sample misalignments of several degrees. A previous study (Abramson et al. 1994) has shown that velocity data can be inverted for both elastic constants and orientations. In the final step of the current data reduction, Euler angles for sample orientations were optimized.

Farnell (1970) treats the general problem of SAW propagation on anisotropic materials. Rayleigh-like surface waves exist for all propagation directions. Pseudo-surface waves (waves that leak acoustic energy into the sample interior) can propagate under more restrictive conditions. The computational procedure developed by Every et al. (1998) is used in the current analysis. The relevant elastodynamic Green's function G_{ij} is evaluated for an impulsive line source stimulation for the experimental geometry (aluminum film over an albite half-space), propagation direction, and assumed elastic constants. The procedure is general and can be applied to any combination of crystal symmetries and orientations. As recommended by Maznev et al. (1999) and further tested by Crowhurst and Zaug (2004), the intensity of the signal was correlated with the modulus of the off-diagonal tensor element $|G_{13}|$; however, re-

sponses calculated with components G_{23} and G_{33} yielded identical peak velocities.

In Fig. 4, acoustic spectra are plotted from an experiment and as calculated from the elastodynamic Green's function for one propagation direction (lab angle of 175° for sample (e) of Fig. 5). The lower frequency peak is the Rayleigh wave for which the theory predicts a delta-function response (the actual peak is off-scale in the plot by two orders of magnitude), while the finite time window of observation results in a broadened Fourier-transform of the experimental record. The higher frequency peak is associated with a pseudo-surface wave; its greater width (in theory and experiment) is appropriate for a wave that is radiating energy into the bulk sample.

Experimental results and reduction to elastic constants

Surface wave velocities obtained on the six oriented and polished surfaces are plotted in Fig. 5 as a function of rotation angle in the plane of each sample. In total, 163 velocities were measured in 125 directions of propagation. The greyscale background in these plots depicts the logarithm of the calculated surface wave response using the optimal set of elastic constants. Lighter shading indicates locations of spectral peaks. We use a "Golden section" algorithm (Press et al. 1986) to determine velocities corresponding to the peaks' maxima. For the optimal set of elastic constants, calculated spectral peaks match the data with an *rms* misfit of 11 m/s.

The velocity data were inverted using both simplex and simulated annealing algorithms (Press et al. 1986) to determine elastic constants. The full set of the optimal elastic constants and their formal uncertainties are given in Table 1. The optimization of triclinic elastic constants from measured surface waves is a non-linear inverse problem. The hyper-space surface which represents the *rms* misfit as a function of all constants contains many local minima, and presents covariances in a search for an absolute minimum. A satisfactory reduction of covariance in calculated constants necessitated a large sample of propagation directions in several crystal surfaces.

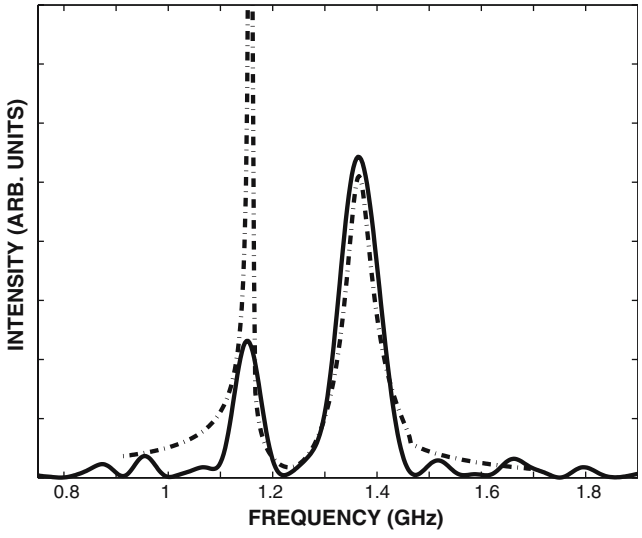

Fig. 4 Surface wave response spectra as a function of frequency at a fixed wavelength of 2.55 μm. The *solid line* is the ISLS spectra for sample (e) (Fig. 5) at an angle of 175°. The *dashed curve* is the calculated $|G_{13}|$ surface wave response for this experimental point

A strength of the current data set is that these velocities are affected by all 21 elastic constants. However, many constants contribute to velocities in any one direction and surface waves, closely related to the transverse body waves, are most sensitive to shear constants. The purely compressional diagonal constants (C_{11}, C_{22}, C_{33}) enter (strongly but not solely) as combinations of differences with non-diagonal elements C_{12}, C_{13}, and C_{23} (e.g. in the simpler case of a cubic crystal, one shear modulus is given by $[(C_{11}-C_{12})/2]$. The six pressure-induced strains from the x-ray compression study are complementary to our sound velocity measurements as they constrain sums rather than differences of the diagonal and non-diagonal constants and are thus particularly useful when combined with the velocity data.

Algorithms for non-linear parameter optimization are not guaranteed to find the global misfit minimum, and we were concerned that more than one combination of elastic constants might predict approximately the same velocities. To additionally validate our solutions, and to more fully explore the elastic constants parameter space, we extensively tested the sensitivity of solutions to assumed initial guesses. Two classes of initial guesses for optimization were used. In an attempt to broadly sample possible combinations of elastic constants, several million sets of random constants were generated. Sets that either did not produce a positive definite elastic matrix or did not meet a loose qualifying misfit constraint based on the moduli from the x-ray study were discarded. The remaining sets were ordered according to the degree of initial misfit to the data, and those with the lowest initial misfit were then selected for optimization. Alternatively, initial guesses were based on the reported monoclinic constants with the remaining triclinic constants all set either to 0, −10, or +10 GPa.

Optimizations often stalled at local minima having unacceptably large values of misfit. In addition to allowing a reduction in uncertainties, the use of constraints provided by the x-ray compression data served to guide the optimization and lessened the probability of being trapped by local minima. We found that optimization on sample orientations could often provide a "tunnel" out of local minima. When the optimizer became trapped, Euler angles were adjusted to reduce misfit for fixed values of elastic constants, then the optimization of constants at fixed orientation resumed. At each point of stalling, the initial guess for orientation optimization was set equal to the x-ray determinations. As the optimizer approached the (likely) global minimum, we found that differences between x-rays determined Euler angles and the optimized Euler angles

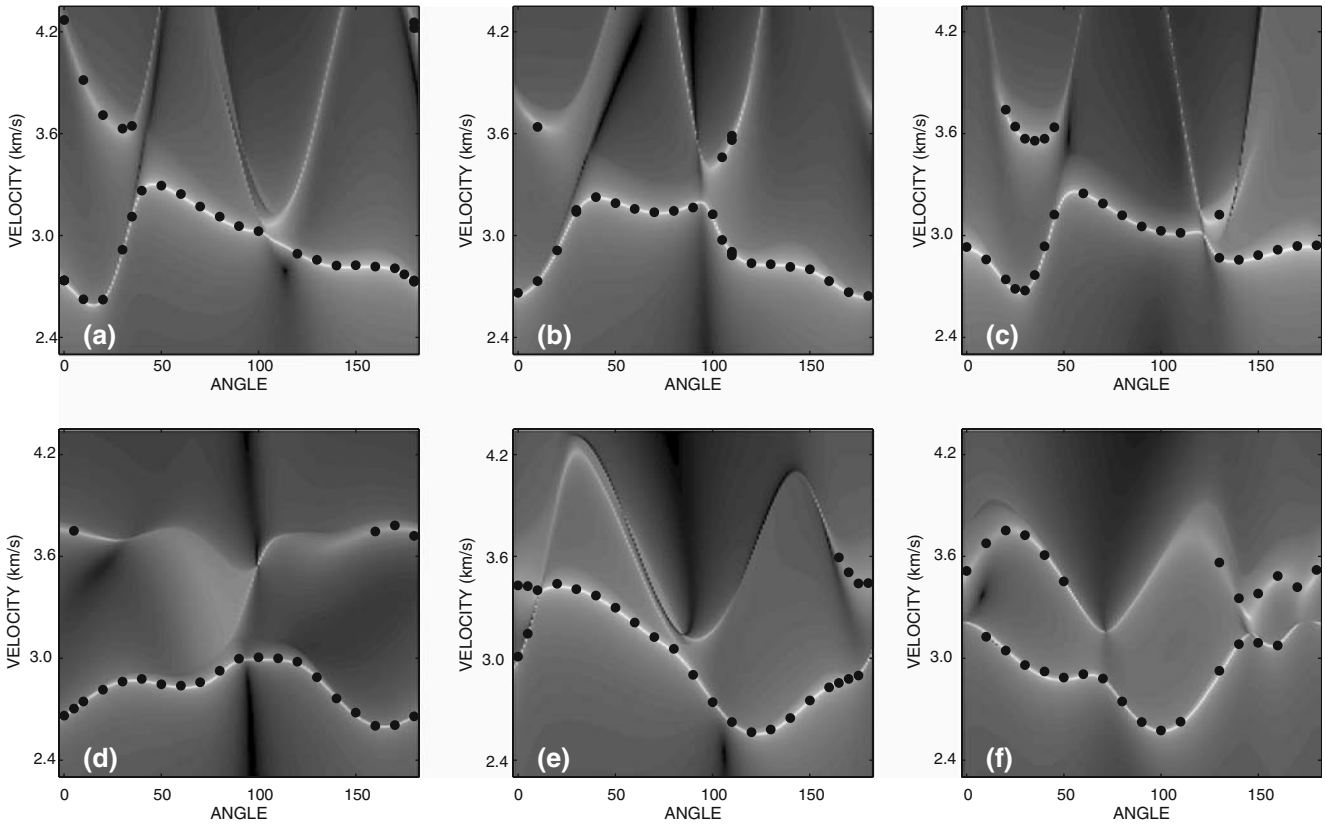

Fig. 5 Measured surface wave velocities (*filled circles*) as functions of laboratory angle about the surface normal and theoretical prediction of surface wave excitation amplitudes (log(|G13|), greyscale background) for the six crystal surfaces. Propagation directions relative to crystal coordinates are shown in stereographic projections in Fig. 3

decreased and were no larger than 3° for the fully optimized constants. Such scatter in orientations is consistent with the expected alignment uncertainty associated with the transfer of the samples from the x-ray goniometer to the optics table. We found that regardless of the optimization algorithm or the choice for initial guesses, optimizations that converged to a misfit, approximately equal to experimental precision, found the same elastic constants to within the reported uncertainties.

Two estimates of uncertainties for the triclinic constants are given in Table 1. In column 7, formal uncertainties calculated using both the surface wave data and the x-ray compression data are given. In the last column uncertainties based solely on SAW velocities are listed. Values larger than about 0.3 GPa are associated with covariance between constants. In particular, the diagonal shears C_{44}, C_{55}, and C_{66} can be well determined from SAW data alone since these constants are dominant in determining velocities in certain directions. Their uncertainties are primarily limited by the uncertainties in measured velocities. On the other hand, none of the constants C_{11}, C_{22}, C_{33}, C_{12}, C_{13}, and C_{23} has a dominant effect on velocities in any one direction of propagation, which results in relatively large covariances in their calculated values. The current data (SAW plus isothermal compliances) could only reduce uncertainties associated with these constants in the range of 0.5–2.7 GPa. Absent the complementary constraint from the x-ray data, uncertainties listed in the last column for the diagonal compressional constants are larger by a factor of 3–5.

In a separate set of Monte Carlo simulations, we confirmed that the formal uncertainty estimates were appropriate and verified that our optimization technique could find the global minimum. Velocities were calculated for the experimental set of propagation directions using the optimal elastic constants. Random noise equal to the expected experimental variance (0.2%) was added. One hundred unique synthetic "data" sets were created (each with its own distribution of errors) and each was fit in the same way as the experimental data. Standard deviations of the elastic constants produced by these Monte Carlo fits were in agreement with the formal uncertainties. Furthermore, constants determined without using the x-ray compliance constraints clustered in the range given by uncertainties in the last column of Table 1.

Discussion

For comparisons with the triclinic data, Ryzhova's monoclinic constants for An_9 were rotated into the

coordinate system of this paper and are listed in the fifth column of Table 1. The averaging of triclinic constants for an aggregate having fully oriented albite and pericline twins leaves the monoclinic constants unchanged with the remaining uniquely triclinic constants being zero. Thus, if correct and neglecting the compositional dependence, the 13 rotated constants should agree with the first 13 constants in the current study. In agreement with Seront et al., a general observation is that many of Ryzhova's constants are smaller, although the diagonal compression constants have the same general trends ($C_{11} < C_{22} \approx C_{33}$). In the current work, C_{22} and C_{33} are nearly 30% larger. Since these constants control compressional velocities along the y and z Cartesian coordinates, the current constants predict 15% higher compressional velocities in these directions. An attempt to find alternate elastic constants that satisfy our surface wave data but have smaller values of C_{22} and C_{33} found only solutions with unacceptably large systematic misfit. We believe that C_{22} and C_{33} are significantly larger than previously reported.

In comparison with Ryzhova's shear elastic constants, several have similar values while C_{23} and C_{35} are the most discordant. We find that these two constants have the most impact in predicting body wave velocities in two directions (the points at 45° in the x-normal and y-normal plots of Fig. 1) where the misfits between Ryzhova's data and predictions are large. Our interpretation is that systematic biases associated with imperfect samples and sparse data led to variable errors in their reported constants.

The pattern of elasticity in albite is consistent with modes of compression determined in the x-ray studies (Downs et al. 1994; Benusa et al. 2005). The constant C_{11} is significantly less than either C_{22} or C_{33}, while the off-diagonal constants involving longitudinal stresses and longitudinal strains have $C_{12} \approx C_{13} > C_{23}$. The dominant mechanism of compression under hydrostatic pressure is the flexing of essentially rigid tetrahedra that results in the closing up of the crankshaft chains of tetrahedra that run along [100], combined with a shearing of the four-rings of tetrahedra that lie parallel to (010). The combined effect of these two mechanisms is to reduce the width of the channels that run parallel to [001] and thus results in the (100) plane normal being the softest direction in the structure. Hence C_{11} is small because compression along the x-axis (100) is accommodated by pure rotation of the stiff tetrahedra. On the other hand, C_{22} and C_{33} are stiffer as a result of the lack of a rotation mechanism to accommodate compression along y or z: compression along y must be accommodated by opening up (or flattening) of the crankshafts and compression along z results in the shearing of the four-rings. The off-diagonal components, C_{13} and C_{12}, are presumably large because compression along x is accommodated almost completely by the compression of the crankshafts without transmission of the strain into the perpendicular directions, whereas C_{23} is small because compression along y must flatten the four-rings parallel to (010) and thus lead to relatively large strains along z.

In Table 3 isotropic averages of the elastic constants for albite are given: (1) as reported in a recent data summary (Hacker and Abers 2004), (2) as calculated from Ryzhova's constants, and (3) as calculated using the triclinic constants reported here. The Voigt values are averages of the constants C_{ij} while the Ruess values are determined from the compliances S_{ij}. The Voigt-Ruess bounds are particularly broad for albite (30% for the shear modulus) as a result of the large anisotropy. The current Hill-average bulk modulus is about 3% larger than Ryzhova's, while the current shear modulus is 24% larger.

Compressional and transverse body wave velocities associated with the triclinic constants are plotted in Fig. 6. The full range of compressional velocity anisotropy between the three axes are shown in the y-normal and z-normal planes. Interestingly, the transverse velocities show less anisotropy in these directions. In the x-normal plane compressional velocities drop from peak values close to the y- and z-axes to minima between the axes. One transverse wave branch has a large anisotropy approaching 3 km/s. In the axis bisecting directions, the polarizations of the longitudinal and transverse wave also become significantly mixed. The differences between these velocities and those predicted by the previously accepted data are large; they are expected to significantly affect analyses of seismic data pertinent to Earth's deep crust.

Conclusions

Velocities of surface acoustic waves were measured on single crystal, low albite. The velocities were inverted to determine the full set of 21 triclinic elastic constants. Results of the current analysis were tested and appear to be robust. This is the first full set of constants reported for any triclinic mineral. Constants, which would be non-zero in the monoclinic case, differ significantly from the pseudo-single crystal results previously reported for the twinned (monoclinic) aggregate. We identify problems that may have caused the earlier work to have biased estimates.

X-ray compressional data provide six important and additional experimental constraints on the elastic con-

Table 3 Isotropic elastic constants for albite as reported by Hacker and Abers (2004), Ryzhova (1964), and as determined in the current work

	V	*H*	*R*	*V*	*H*	*R*
Hacker and Abers		54			28	
Ryzhova	62	57	53	31	29	27
Current work	64	60	55	41	36	30

The mean of the Voigt average (V) and the Ruess average (R) is the Hill average (H). Bulk Modulus (GPa) and Shear Modulus (GPa)

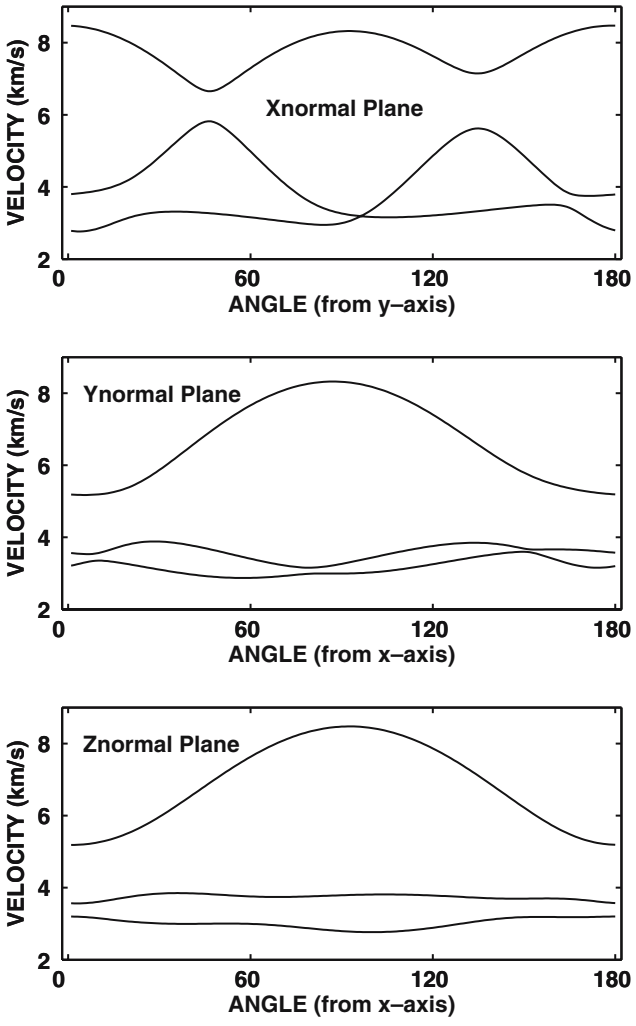

Fig. 6 Longitudinal and transverse body wave velocities for albite. The three panels show velocities in three orthogonal planes

stants. As the surface wave velocity data typically constrain differences of diagonal and off-diagonal constants, while the compressional data constrain sums, the two studies complement each other and together provide greatly reduced uncertainties.

Acknowledgements We thank Scott Pendleton and Edward Chang who prepared samples and made the velocity measurements as part of an undergraduate research experience degree requirement. We thank Bernard Evans (who collected and provided the albite samples), Arthur Every (who graciously provided the surface wave code PANGIM), Scott Kuener (who made the microprobe analysis), and Jason Benedict (who made the x-ray orientations with assistance from Werner Kaminsky). We thank Robert Downs who provided assistance in interpreting x-ray orientation data and in confirming our orientations. R.L. Carlson and N.I. Christensen are acknowledged for discussions that have extended over many years concerning feldspars. We thank David Mainprice for discussions. Jonathan Crowhurst is acknowledged for discussions on appropriate choices for the Green's function elements. Suggestions by the reviewers also improved the manuscript. This work was partially funded with NSF support through grants EAR 0106683, EAR 0221404 (JMB and EHA) and EAR 0408460 (RJA).

Appendix

The general framework of elasticity notation is reviewed and the Voigt contraction convention is defined in Nye (1969). Elements of the infinitesimal strain (ε) and stress (σ) tensors are expressed in terms of Cartesian axes ($1 = x$, $2 = y$, $3 = z$). The first index indicates the direction of displacement of (or force acting on) a plane normal to the direction of the second index. Thus, ε_{11} is longitudinal strain consisting of a displacement along the x-axis of the yz plane, while the shear strain ε_{12} indicates movement in the x direction of a plane normal to y. In the contracted Voigt notation the 11, 22, and 33 elements of the stress or strain tensors are referred to as 1, 2 and 3, while the off-diagonal elements 23, 13, and 12 are, respectively, 4, 5, and 6. Thus, the fourth-order elastic constants tensor, C_{ijkl} that maps strains into stresses, can be contracted into a 6×6 matrix. The diagonal constants C_{11}, C_{22}, and C_{33} map longitudinal strains into the parallel longitudinal stresses, while C_{12}, C_{13}, and C_{23} map longitudinal strains onto longitudinal stresses in orthogonal directions. Constants C_{14}, C_{15}, C_{16}, C_{24}, C_{25}, C_{26}, C_{34}, C_{35}, and C_{36} map longitudinal strains into shear stresses. The remaining constants (C_{44}, C_{55}, C_{66}, C_{45}, C_{46}, C_{56}) map shear strains into shear stresses.

References

Abramson EH, Slutsky LJ, Brown JM (1994) Elastic constants, interatomic forces, and equation of state of β—oxygen at high pressure. J Chem Phys 100:4518–4526

Abramson EH, Brown JM, Slutsky LJ (1999) Applications of impulsive stimulated scattering in the earth and planetary sciences. Ann Rev Phys Chem 50:279–313

Aleksandrov KS, Alchikov UV, Belikov BP, Zalavskii BI, Krupnyi AI (1974) Velocities of elastic waves in minerals at atmospheric pressure and increasing precision of elastic constants by means of EVM Izv. Acad Sci USSR Geol Ser 10:15–24

Babuska V (1981) Anisotropy of V_p and V_s in rock-forming minerals. J Geophys-Zeitschrift Fur Geophysik 50:1–6

Bass JD (1995) Elasticity of minerals, glasses, and melts. In: Ahrens TJ (ed) Mineral physics and crystallography. A handbook of physical constants. (AGU reference shelf 2) AGU, Washington DC, pp 45–63

Benusa MD, Angel RJ, Ross NL (2005) Compression of albite, $NaAlSi_3O_8$. Am Mineral 90:1115–1120

Brown JM, Slutsky LJ, Nelson KA, Cheng LT (1989) Single-crystal elastic constants for San Carlos Peridot; an application of impulsive stimulated scattering. J Geophys Res 94:9485–9492

Carlson RL, Miller DJ (2004) Influence of pressure and mineralogy on seismic velocities in oceanic gabbros: implications for the composition and state of the lower oceanic crust. J Geophys Res 109:B09205

Christensen NI (1996) Poisson's ratio and crustal seismology. J Geophys Res 101:3139–3156

Christensen NI, Fountain DM (1975) Constitution of lower continental crust based on experimental studies of seismic velocities in granulite. Geol Soc Am Bull 86:227–236

Crowhurst JC, Zaug JM (2004) Surface acoustic waves in germanium single crystals. Phys Rev B 69:52301-1-4

Downs RT, Hall-Wallace M (2003) American mineralogist crystal structure database. Am Mineral 88:247–250

Downs RT, Hazen RM, Finger LW (1994) The high-pressure crystal chemistry of low albite and the origin of the pressure dependency of Al-Si ordering. Am Mineral 79:1042–1052

Every AG, McCurdy AK (1992) Numerical data and functional relationships in science and technology. In: Madelung O (ed) Landoldt-Börnstein, new series, group III. Springer, Berlin Heidelberg New York

Every AG, Kim KY, Maznev AA (1998) Surface dynamic response functions of anisotropic solids. Ultrasonics 36:349–353

Farnell GW (1970) Properties of elastic surface waves. In: Mason WP, Thurston RN (eds) Physical Acoustics. Academic, New York, pp 109–166

Fountain DM, Salisbury MH, Percival J (1990) Seismic structure of the continental-crust based on rock velocity-measurements from the Kapuskasing uplift. J Geophys Res 95:1167–1186

Hacker BR, Abers GA (2004) Subduction factory 3: an excel worksheet and macro for calculating the densities, seismic wave speeds, and H_2O contents of minerals and rocks at pressure and temperature. Geochem Geophys Geosys 5. DOI 10.1029/2003GC000614

Hacker BR, Abers GA, Peacock SM (2003) Subduction factory-1. Theoretical mineralogy, densities, seismic wave speeds, and H_2O contents. J Geophys Res 108. DOI 10.1029/2001JB001127

Harlow GE, Brown G (1980) Low albite: an X-ray and neutron diffraction study. Am Mineral 65:986–995

Haussuhl S, Siegert H (1969) Determination of elasticity tensor of triclinic crystals—example $CuSO_{4.5}H_20$. Z Kristallogr Kristallgeom Kristallphys Kristallchem 129:142–146

Kroll H, Ribbe P (1983) Lattice parameters, composition and Al, Si order in alkali feldspars. In: Ribbe P (ed), Feldspar mineralogy (Reviews in mineralogy). Miner Soc Amer, Washington DC, pp 57–98

Kuppers H, Siegert H (1970) Elastic constants of triclinic crystals ammonium and potassium tetroxalate dihydrate. Acta Crystallogr A A26:401–405

Liebermann RC, Ringwood AE (1976) Elastic properties of anorthite and nature of lunar crust. Earth Planet Sci Lett 31:69–74

Maznev AA, Akthakul A, Nelson KA (1999) Surface acoustic modes in thin films on anisotropic substrates. J Appl Phys 86:2818–2824

McDonough DT, Fountain DM (1988) Reflection characteristics of a mylonite zone based on compressional wave velocities of rock samples. Geophys J 93:547–558

Navrotsky A (1995) Thermodynamics properties of minerals. In: Ahrens TJ (ed), Mineral physics and crystallography: a handbook of physical constants. (AGU reference shelf 2) AGU, Washington DC, pp 18–28

Nye JF (1969) Physcial Properties of crystals, their representation by tensors and matrixes. Oxford, Clarendon Press, p 322

Peselnick L, Nicolas A (1974) Velocity anisotropy in a mantle peridotite from Ivrea zone—application to upper mantle anisotropy. J Geophy Res 79:1175–1182

Press WH, B. Flannery S. Teukolsky, Vettering W (1986) Numerical recipes. Cambridge University Press, New York

Ryzhova TV (1964) Elastic properties of plagioclases. Akad SSSR Izv Ser Geofiz 7:1049–1051

Salisbury MH, Christensen NI (1978) Seismic velocity structure of a traverse through Bay of Islands Ophiolite complex, Newfoundland, an exposure of oceanic-crust and upper mantle. J Geophys Res 83:805–817

Salisbury MH, Fountain DM (1994) The seismic velocity and poissons ratio structure of the Kapuskasing uplift from laboratory measurements. Can J Earth Sci 31:1052–1063

Schlenker JL, Gibbs GV, Boisen MB Jr (1978) Strain-tensor components expressed in terms of lattice parameters. Acta Crystallogr A A34:52–54

Seront B, Mainprice D, Christensen NI (1993) A determination of the 3-dimensional seismic properties of anorthosite—comparison between values calculated from the petrofabric and direct laboratory measurements. J Geophys Res 98:2209–2221

Takanashi M, Nishizawa O, Kanagawa K, Yasunaga K (2001) Laboratory measurements of elastic anisotropy parameters for the exposed crustal rocks from the Hidaka metamorphic belt, Central Hokkaido, Japan. Geophys J Int 145:33–47

Winter JK, Ghose S, Okamura FP (1979) A high-temperature study of the thermal expansion and the anisotropy of the sodium atoms in low albite. Am Mineral 62:921–931